

## EXCITED STATE PROPERTIES CALCULATIONS: FROM 0 TO 3 DIMENSIONAL SYSTEMS

M. MARSILI <sup>(1)</sup>, V. GARBUIO <sup>(1)</sup>, M. BRUNO <sup>(1)</sup>, O. PULCI <sup>(1)</sup>, M.  
PALUMMO <sup>(1)</sup>, E. DEGOLI <sup>(2)</sup>, E. LUPPI <sup>(3)</sup>, R. DEL SOLE <sup>(1)</sup>

<sup>(1)</sup> *ETSF and INFM and Dipartimento di Fisica dell'Università di Roma Tor Vergata, via della Ricerca Scientifica, I-00133 Roma, Italy*

<sup>(2)</sup> *INFM-S<sup>3</sup> "nanoStructures and bioSystems at Surfaces", Dipartimento di Scienze e Metodi dell'Ingegneria, via G. Amendola 2, Università di Modena e Reggio Emilia*

<sup>(3)</sup> *ETSF and Laboratoire des Solides Irradiés, École Polytechnique, F-91128 Palaiseau, France*

We review the theoretical framework of *ab-initio* excited state properties calculations showing the application of these methods to systems of different dimensionality. Density functional theory within the usual and generalised Kohn-Sham scheme is presented and applied to the case of the cleavage surface of diamond. Many body perturbation theory within the GW approximation of the self energy for the calculation of electronic band structures is presented and applied to liquid water. Finally, the Bethe Salpeter equation for the computation of optical properties is presented and used for the case of silicon nanowires and silicon nanoclusters

### 1. Introduction

Many experimental techniques in solid state physics, such as angle resolved photoemission spectroscopy (ARPES), electron energy loss (EELS), optical absorption etc... probe the electronic excitations of the systems under investigation. As a consequence a material is often characterised by its excited state properties. A completely *ab-initio*, parameter free, determination of the excited state properties of materials is thus very important for the interpretation of the experimental spectra and/or for the prediction of the material's features. In this paper we will review the well established theoretical background of the *state of the art* calculation of excited state properties and we will show how these methods can be applied to systems of different dimensionality.

All the calculations presented in this paper are performed using codes<sup>1</sup>

that employ plane wave basis set. This kind of basis set allows for the intensive use of fast algorithms such as fast Fourier transforms (FFT) and moreover allows a systematic check on the convergency of the calculation. Of course plane waves are suited to describe crystal bulk systems in which a certain unit cell is repeated in all the three directions in space. However as we will show below, also lower dimensionality systems such as surfaces, nanowires, and molecules and even disordered systems such as liquid water can be studied within the same scheme. Of course in all these cases special care has to be put in order to avoid spurious effects due to the infinite reproduction of the unit cell, the so called *supercell*. In the case of a surface, the supercell is made by a certain amount of atomic layers meant to reproduce the bulk and the surface of the system and by a certain amount of vacuum. When this supercell is repeated in all the three directions in space the resulting system is given by a infinite series of repeated slabs. To obtain well converged results the vacuum must be deep enough so that the slabs are decoupled, and there must be enough atomic layers so that the bulk is well represented. Also in the case of nanowires, molecules and nanoclusters the final geometry consists of an infinite series of repeated replicas of the system. Like in the case of surfaces, the convergency with respect to the amount of vacuum present between them must be carefully checked. Especially in the calculations of excited state properties, where the electronic empty states play an important role, it might be very convenient to use spherical<sup>4</sup> (for molecules and nanoclusters) or cylindrical<sup>5,6</sup> (for nanowires) cutoff functions for treating the long range term of the Coulomb interaction. The peculiar problem related to the study of a liquid disordered system relies on the fact that one should in principle use a very large unit cell. A possible solution to avoid such huge unit cells has been proven<sup>7</sup> to be the use of smaller unit cells but exploiting several molecular dynamics (MD) snapshots of water as input geometries and averaging the results over all the configurations.

The paper is organised as follows: first, ground state calculations within density functional theory (DFT), preliminary to all the excited state calculations will be presented; as an example we will show the calculations for the (111)2×1 surface of diamond. Then, we will see how quasiparticle effects can be introduced to get a reliable description of the electronic band structure and we will see how this method is applied to the case of liquid water. Finally we will see how many body effects, such as the excitonic effects, can be introduced in the calculations of optical spectra, and we will show the results of calculations for silicon nanowires and a small silicon

nanocluster.

## 2. Determination of the ground state: C(111)2 × 1

As already mentioned, the computation of the excited state properties is based on a previous well converged ground state calculation. Here we schematically review the theory behind this kind of calculations and show the application for the cleavage surface of diamond.

Within the the Born-Oppenheimer approximation the electronic Hamiltonian of a system of interacting electrons in an external potential is given by

$$H = \sum_i -\frac{1}{2}\nabla_{\mathbf{r}_i}^2 + V_{ext} + \frac{1}{2} \sum_{i,j}^i \frac{1}{|\mathbf{r}_i - \mathbf{r}_j|} = T + V_{ext} + V_{e-e}. \quad (1)$$

Even though the ions coordinates appear just as parameters in  $V_{ext}$ , eq. (1) is still very involved and a direct diagonalisation to find its eigenstates is still a formidable task that for complex systems is out of the reach of the computational power. The density functional approach, focusing the attention on the *simpler* total electronic density  $n(r)$  rather than on the more complex many body wavefunction  $\Psi(r_1, \dots, r_N)$ , opens the way to the study of the ground state properties of even very complex systems.

Density Functional Theory (DFT) treats the case of an external, time independent potential, and is based on the seminal paper of Hohenberg and Kohn of 1964<sup>8</sup>. For a review on DFT see for example<sup>9</sup>. The Hohenberg and Kohn theorem states that once the mutual interaction among the electrons is fixed, in a non time dependent situation and assuming that all the potentials acting on the system are local, all the ground state properties of an interacting electronic system, including, in principle, the many-body wave function, could be expressed as unique functionals of the electronic density alone. In particular this assertion is valid also for the total energy  $E$  of the system. For the total energy functional  $E[n]$ , a variational principle could be derived stating that for a given density  $n(\mathbf{r})$

$$E[n(\mathbf{r})] = F[n] + \int d\mathbf{r} V_{ext}(\mathbf{r})n(\mathbf{r}) \geq E_{GS} \quad (2)$$

where  $E_{GS}$  is the ground state energy of the system, and  $F[n] = T + V_{ee}$  is a universal functional that contains the contribution of the kinetic ( $T$ ) and electron-electron ( $V_{ee}$ ) part of the hamiltonian. In particular the energy functional finds its minimum at the ground state density  $E[n_{GS}] = E_{GS}$ . This theorem leads, in principle, to a straightforward method for computing

ground state properties: given an approximation for the functional dependence of  $F$ , the ground state density can be obtained by a minimisation procedure of the energy functional, and then, knowing the functional dependence on the density of the properties of interest, one can find their ground state value. However finding a suitable approximation for  $F$  is a formidable and very delicate task. In fact, beside the contribution of the electron-electron interaction, most of which usually can be included in the Hartree term,  $F$  contains the kinetic energy whose functional dependence on the density is unknown and, most important, it constitutes a non negligible part of the total energy. This means that an approximation made directly on this term can lead to big errors in the total energy of the system.

The breakthrough appeared one year later, with the paper of Kohn and Sham<sup>10</sup> (KS) where they introduced a different separation of the terms contributing to the total energy  $E$ . The two main advantages of this separation were first of all to provide a single particle (selfconsistent) scheme to obtain the groundstate density and total energy, and second, but still very important, to have an expression in which the approximation of the unknown part would be, in many cases, not as relevant as before. In the KS scheme the total energy functional is written as:

$$E[n] = T_0[n] + E_H[n] + \int d\mathbf{r} n(\mathbf{r}) v_{ext}(\mathbf{r}) + E_{xc}[n] \quad (3)$$

$T_0$  is the kinetic energy of a non interacting system with density  $n$ ,  $E_H$  is the Hartree contribution to the total energy, and  $E_{xc}$  is the remaining part of the total energy which contains exchange-correlation contributions plus the difference between the kinetic energy of the non interacting system  $T_0$  and the true kinetic energy  $T$ . Given this form for the total energy functional it can be shown that the system of interacting electrons will have the same density of a system of non interacting electrons subject to an effective potential given by  $v_{KS} = v_{ext} + v_H + v_{xc}$  where  $v_{xc} = \frac{\delta E_{xc}[n]}{\delta n(\mathbf{r})}$ . Now for the auxiliary system of non interacting electrons a single particle Schrödinger equation can be written:

$$\left[-\frac{1}{2}\nabla^2 + v_{ext} + v_H + v_{xc}\right]\phi_i(\mathbf{r}) = \varepsilon_i \phi_i(\mathbf{r}) \quad (4)$$

so that the ground state density of the interacting system is expressed in terms of single KS orbitals:

$$n(r) = \sum_i f_i |\phi_i(\vec{r})|^2 \quad (5)$$

where  $f_i$  is the occupation number of the state  $i$ . It is now possible, given an approximation for  $v_{xc}[n]$ , to solve the Kohn-Sham equations (4),(5) selfcon-

sistently and hence to calculate the density of the interacting (real) system. Once the density is known, it is possible to calculate the energy of the ground state of the interacting system and hence, by proper minimisation, to find the ground state geometry of the (real) system. The simplest and most common approximation to  $E_{xc}$  is the Local Density Approximation LDA given by<sup>10</sup>:

$$E_{xc}^{LDA} = \int d\mathbf{r} n(\mathbf{r}) \epsilon^{\text{heg}}(n(r)) \quad (6)$$

where  $\epsilon^{\text{heg}}(n)$  is the exchange-correlation energy per electron of a homogeneous electron gas of density  $n$ . A possible way to go beyond LDA is to introduce an energy functional that depends also on the derivative of the density, the so called generalised gradient approximation (GGA) functionals<sup>11,12</sup>. Otherwise, as shown in ref.<sup>13</sup>, partitioning the total energy functional in a different way with respect to the Kohn Sham decomposition given by eq. (3), one can still retain a single particle equation scheme, but exactly treat important portions of the exchange and correlation energies. In the calculation of total energies, these *generalised Kohn-Sham* schemes present the same accuracy as the original Kohn and Sham one. However, as we will discuss in more detail later, if one is interested in interpreting the KS eigenvalues as addition and removal energies, these latter schemes seem to yield results closer to experimental values.

As an example of ground state calculation we show here the results for the (111)2×1 surface of diamond. From a theoretical point of view, this surface is very interesting because the electronic structure depends strongly on the details of the geometry of its reconstruction. Experimentally, right after cleavage, the (111) surface of diamond exhibits a 1×1 periodicity. After annealing at more than 1000 K, however, hydrogen desorbs and the surface undergoes a 2×1 reconstruction. Both experiments and theory up to now agree that the reconstruction geometry is the Pandey chain model<sup>14</sup>, but the details of the relaxation, i.e. dimerisation or buckling of the surface chains, are still not fully experimentally clarified. The exact determination of these details is important because, at the DFT level, the existence and the magnitude of the gap between surface states depend on them<sup>15</sup> in such a way that it is still not clear whether the experimentally observed semiconducting character of this surface is due to some geometrical deviations from the ideal Pandey chain model or, instead, to quasiparticle effects. Here we will show the results concerning the ground state geometry of this surface. Then we will see how deviations from this geometry can influence the band

structure. We will employ both Kohn-Sham and generalised Kohn-Sham schemes to see if also in this case the latter yields a better agreement with experimental results. Unfortunately both schemes fail to reproduce the experimentally found semiconducting character of the surface.

The surface was modelled using a repeated slab made of 12 atomic layers of carbon atoms plus  $\sim 5.4\text{\AA}$  of vacuum. The initial ionic positions were changed from the ideal position breaking all the possible symmetries of the ideal lattice except for the inversion of the  $z$  axis; all the atomic layers were allowed to move except for the central 2 layers. In the optimisation of the geometry we started from several configurations, involving Pandey chains with buckling and dimerisation. In the calculation we used different kind of functionals LDA and GGA. The final relaxed geometry, common to all the starting points, is shown in Fig.1.

We find that the buckling and the dimerisation of the chains vanish, thus

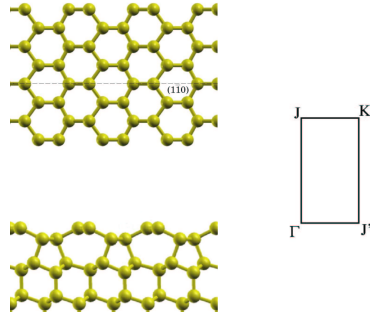


Figure 1. Pandey chain model for the  $(111) 2 \times 1$  surface of diamond. (Top view in the top panel, side view in the bottom panel). The reconstruction involves a significant change in the lattice structure. The irreducible Brillouin zone and its high symmetry points are also shown.

confirming previous DFT-LDA results<sup>16,17</sup>.

The resulting electronic band structure is semimetallic in contrast with experimental data that predict a gap of at least  $0.5\text{ eV}$ <sup>18</sup>. In particular, as we can see in Fig.2, where the DFT-GGA band structure is presented, the surface states, labelled as  $N$  and  $N + 1$ , are crossing the Fermi level along the JK line. Besides this, the agreement with the experimental dispersion of the occupied state is remarkably good.

However, it is known that the interpretation of DFT KS eigenvalues as addition and removal energies is not theoretically established<sup>20</sup>. The qualitative agreement with the experimental spectra is often very good but the

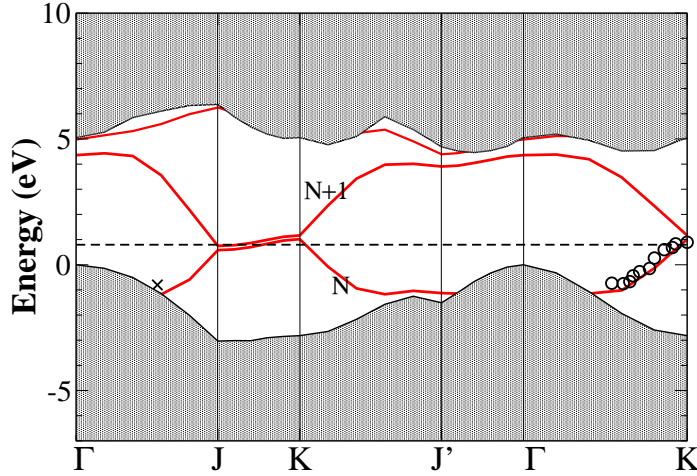


Figure 2. Electronic band structure of the  $2 \times 1$  surface. In agreement with previous DFT calculation the surface is semimetallic. Between J and K the upward dispersion of the surface bands, due to the interaction between different chains, makes both the surface bands cross the Fermi level (dashed line). All the energies are referred to the top of the valence band. Circles: experiments from <sup>18</sup>; crosses: experiment from. <sup>19</sup>

band gaps are systematically underestimated. This could be the origin of the qualitative disagreement with experiment found for the C(111) surface. In fact the DFT KS gap  $E_g^{DFT}$  of the  $N$  particle system, is related to the *true* quasiparticle gap through the discontinuity  $\Delta$  of the exchange and correlation potential when an electron is added to the system.

$$E_g = E_g^{KS} + \Delta = \epsilon_{N+1}^{(N)} - \epsilon_N^{(N)} + v_{xc}^+ - v_{xc}^- \quad (7)$$

Where  $\epsilon_{N'}^{(N)}$  represents the  $N'$ -th single particle Kohn-Sham level in a  $N$ -particle calculation. Now, if  $\Delta$  is very small, a functional good enough would provide the correct gap; viceversa, if  $\Delta$  is a big quantity, no matter how good the functional is, the Kohn Sham gap does not provide a good approximation for the quasiparticle gap. The discontinuity of the exchange and correlation potential was found<sup>20</sup> to be a consistent (80%) part of the error, the quasiparticle gap problem should then be addressed within different theories or schemes.

In the generalised Kohn-Sham schemes using hybrid functionals such as screened exchange (sX) the discontinuity of the exchange correlation potential is already partly incorporated in the single particle eigenstate of the system<sup>13</sup>. This fact yields reasonably good description of the electronic

band structures of semiconductors, yielding gaps larger than the Kohn-Sham ones, but often smaller than the experimental gaps. As we will see in the next section, the problem of addition and removal energies can be directly addressed within many body perturbation theory (MBPT), through the introduction of quasiparticle effects, within the GW scheme<sup>24,22,23</sup>.

In the case of the (111) surface of diamond we have tried to see if the generalised schemes would recover at least a qualitative agreement with experiments. We relaxed the surface geometry using the sX and Hartree Fock hybrid functionals. In all cases no buckling nor dimerisation was present in the final relaxed geometry, and the surface stayed semimetallic, as we can see from Fig.3

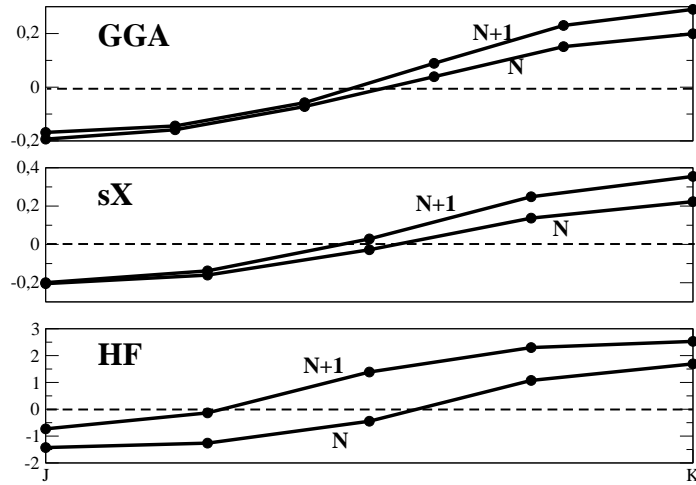


Figure 3. Surface states energies along the JK line, within the GGA, sX, and Hartree Fock schemes, for the equilibrium geometry (no buckling, no dimerisation). In all cases the surface is semimetallic. All energies are in eV and referred to the Fermi level.

### 3. Quasiparticle effects in the electronic band structure

Density Functional Theory, presented in the previous section, is a very powerful tool to study ground state properties of electronic systems. Within this theory the Kohn Sham eigenvalues are introduced as Lagrange multipliers, so that their interpretation as excitation energies of the real system has no theoretical foundation. In fact their interpretation as excitation energies leads to the well known band gap problem of DFT: the band gaps

predicted by the theory are typically 30-50% (sometimes even more) smaller than the experimental ones.

The theoretical framework that is most appropriate to treat excited state properties of many particle systems is the Green's function theory. The single particle Green's function is defined as

$$G(1, 2) = -i \langle N | \mathcal{T} \{ \hat{\psi}(1) \hat{\psi}^\dagger(2) \} | N \rangle, \quad (8)$$

where  $|N\rangle$  is the ground state of a  $N$  particles system,  $\mathcal{T}$  is the time ordering operator,  $\hat{\psi}(i)$  ( $i = 1, 2$ ) is a field operator in the Heisenberg picture, the index  $i$  represents the position  $\mathbf{r}_i$ , spin  $\sigma_i$  and time  $t_i$  coordinate, while  $x_i$  includes both the position and the spin coordinates of the  $i$ -th particle. If we Fourier transform with respect to time we obtain the Lehmann representation of the Green's function given by:

$$G(x_1, x_2, \omega) = \sum_s \frac{f_s(x_1) f_s^*(x_2)}{\omega - \epsilon_s - i\eta \text{sgn}(\mu - \epsilon_s)}, \quad (9)$$

here  $\mu$  is the Fermi energy of the system,  $s$  runs over the  $(N+1)$  or  $(N-1)$  particles excited states and

$$\begin{cases} f_s(x_i) = \langle N | \hat{\psi}(x_i) | N+1, s \rangle \text{ and } \epsilon_s = E(N+1, s) - E(N) \text{ when } \epsilon_s > \mu \\ f_s(x_i) = \langle N-1, s | \hat{\psi}(x_i) | N \rangle \text{ and } \epsilon_s = E(N) - E(N-1, s) \text{ when } \epsilon_s < \mu \end{cases} \quad (10)$$

In this representation it can be seen that the poles of the Green's function are exactly the electron addition and removal energies. However, while shading light on the physical information contained in the single particle Green's function, the Lehman representation is not very useful in practice. Instead for low energies excitations and analytically continuing the Green's function in the plane of complex frequencies, a single-particle like framework can be regained introducing the concept of quasiparticles (QP). Quasi-particles can be thought as the original particles surrounded by an electron-hole polarisation cloud that screens their mutual interaction. QP are not eigenstates of the real Hamiltonian and have finite lifetimes.

The dynamic of the QPs is accounted for the self-energy operator,  $\Sigma$ . It is a non-local, non-hermitian, energy-dependent operator which includes the Fock exchange and all the remaining correlation effects so that QPs obey a Schrödinger-like equation similar to equations (4) of DFT:

$$H_0 \psi_n(x, \omega) + \int dx' \Sigma(x, x', \omega) \psi_n(x', \omega) = E_n(\omega) \psi_n(x, \omega), \quad (11)$$

where  $H_0(x_1) = -\frac{1}{2}\nabla^2 + v_{ext} + v_H$ .

It can be shown that the QP equation 11 is equivalent to the Dyson equation:

$$G(1, 2) = G_0(1, 2) + \int d(34) G_0(1, 3)\Sigma(3, 4)G(4, 2), \quad (12)$$

The Dyson equation connects the interacting Green's function  $G$  to the Green's function of the system subject only to  $H_0$

It can also be shown that  $G$  and  $\Sigma$  are fully determined by a close set of equations derived by Hedin<sup>24</sup> in 1965:

$$\Sigma(1, 2) = i \int d(34) G(1, 3)\Gamma(3, 2, 4)W(4, 1^+); \quad (13)$$

$$\Gamma(1, 2, 3) = \delta(1, 2)\delta(1, 3) + \int d(4567) \frac{\delta\Sigma(1, 2)}{\delta G(4, 5)} G(4, 6)G(7, 5)\Gamma(6, 7, 3) \quad (14)$$

$$P(1, 2) = -i \int d(34) G(1, 3)G(4, 1^+)\Gamma(3, 4, 2); \quad (15)$$

$$W(1, 2) = V(1, 2) + \int d(34) W(1, 3)P(3, 4)V(4, 2); \quad (16)$$

where  $1^+$  stands for  $(\mathbf{r}_1, \sigma_1, t_1 + \delta)$ ,  $\delta$  is an infinitesimal positive number,  $P(1, 2)$  the time ordered polarisation operator,  $W(1, 2)$  the dynamical screened Coulomb interaction and  $\Gamma(1, 2, 3)$  is the vertex function.

Hedin's equations together with the Dyson's one for the Green's function form a set of equations that must be solved self-consistently. This leads in principle to the exact solution of the many-body problem, but it is practically impossible for realistic systems so that these equations are typically solved using an iterative scheme. Concerning the determination of  $\Sigma$ , the simplest approximation consists in starting with a non-interacting system by putting  $\Sigma = 0$ ; in this case the Green's function is simply  $G_0$ , the vertex corrections are neglected with  $\Gamma(1, 2, 3) = \delta(1, 2)\delta(2, 3)$  and the irreducible polarisability is given by non-interacting electron hole pairs  $P(1, 2) = -iG_0(1, 2)G_0(2, 1^+)$ . With this first iteration step the self-energy becomes

$$\Sigma(1, 2) = iG_0(1, 3)W_0(3, 1); \quad (17)$$

that is the so-called GW approximation, first introduced by Hedin<sup>24</sup> in 1965.

In practice, thanks to the similarity of equations (11) and (4) the problem is treated in a perturbative way with respect to the difference between the

self-energy and the Kohn and Sham exchange-correlation potential. At the first order, the quasiparticle energies are

$$E_n = \varepsilon_n + \langle \phi_n^{KS} | \Sigma(E_n) - v_{xc}^{KS} | \phi_n^{KS} \rangle. \quad (18)$$

The usual way to proceed is to expand the self-energy to first order around  $\varepsilon_n$ :

$$\langle \Sigma(E_n) \rangle = \langle \Sigma(\varepsilon_n) \rangle + (E_n - \varepsilon_n) \left\langle \frac{\partial \Sigma(\omega)}{\partial \omega} \right\rangle_{\omega=\varepsilon_n} + \dots \quad (19)$$

and calculate the GW corrections to the Kohn and Sham energies:

$$E_n - \varepsilon_n = \frac{\langle \Sigma(\varepsilon_n) \rangle - \langle v_{xc}^{KS} \rangle}{1 - \left\langle \frac{\partial \Sigma(\omega)}{\partial \omega} \right\rangle_{\omega=\varepsilon_n}}. \quad (20)$$

This is the standard GW approximation that typically yields quite accurate results for one-particle excitations removing the underestimation of the band gap, peculiar of DFT.

### 3.1. *Example: liquid water*

As an example of GW calculation in complex systems, we show the results obtained within this theory for a particular three dimensional system: liquid water<sup>7</sup>. As already mentioned, to avoid the use of very large supercell we use several MD snapshots of water as input geometries and averaged the results. We used 20 configurations of 17 water molecules in a cubic box with 15 a.u. side. We firstly used DFT to obtain Kohn-Sham eigenvalues and eigenvectors and then corrected the energy levels within the GW approximation. In the calculations we used GGA pseudopotentials and 8 k-points to sample the Brillouin zone. DFT-KS results for the electronic properties of water (obtained averaging over the 8 k points for each of the 20 configurations) are shown in Fig.4. The configuration-averaged HOMO-LUMO gap turned out to be 5.09 eV, in good agreement with previous DFT calculations<sup>25</sup> but strongly underestimating the experimental gap (8.7 ± 0.5 eV<sup>26</sup>), as expected in DFT.

In order to correct the KS electronic gap we calculated the GW corrections  $\Delta \varepsilon_n^{QP}$  to the KS energies. This should be done for *all* the 20 MD configuration, followed by an average. In particular the calculation of the screened Coulomb interaction for 20 configurations constitutes a true bottleneck. Instead, we observed that the GW corrections  $\Delta \varepsilon_n^{QP}$  were quite stable with respect to the configuration. In other words, the difference between DFT and GW,  $\Delta GW = \varepsilon_n^{QP} - \varepsilon_n^{DFT}$ , was practically constant going

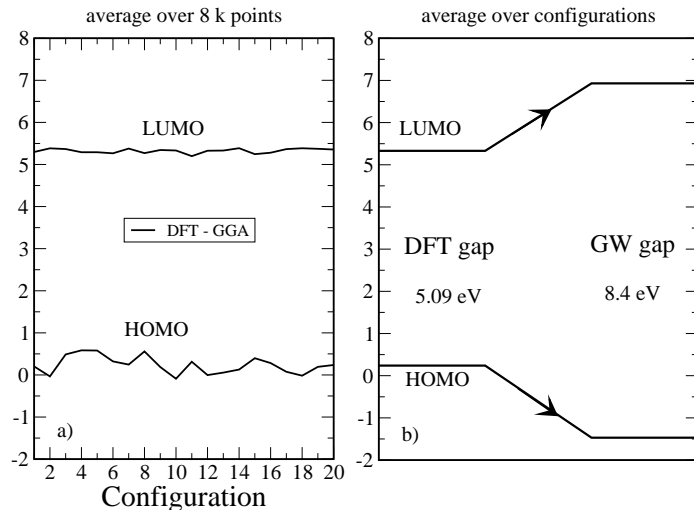


Figure 4. a) DFT HOMO and LUMO energies, averaged over the 8 k-points, for the 20 MD configurations. b) Schematic DFT and GW HOMO-LUMO gaps, averaged over the 20 MD configurations.

from one snapshot to another. This is explicitly shown in table 1 for three different configurations. We used, hence, the same GW corrections for all the DFT configurations.

Table 1. GW corrections to the HOMO and LUMO energy levels and to the GGA electronic gap, for three different water configurations (E19, E8, E2). Energies in eV.

	DFTgap	$\Delta GW$ HOMO	$\Delta GW$ LUMO	$\Delta GW$ gap
E19	5.09	-1.67	1.61	3.28
E8	4.71	-1.64	1.60	3.24
E2	5.29	-1.70	1.60	3.30

With this GW corrections the average electronic HOMO-LUMO gap is increased to 8.4 eV well within the experimental range<sup>26</sup>, as shown in Fig.4.

#### 4. Many body effects in the optical properties

The application of the approach described in the previous section yields, in many cases, to energy levels in good agreement with photoemission and inverse photoemission experiments in semiconductors, insulators and metals<sup>27</sup>. In this kind of experiment the system is left in a charged excited state

where the electron is removed or added to system. On the other hand, in order to describe correctly the spectroscopic processes, where electron–hole pairs are created, the inclusion of solely the self-energy corrections to the DFT eigenvalues in the RPA formula for the polarisation  $P$  (which is the key quantity to obtain the measured spectra), is still not enough. In fact it is not possible to stop at the independent particle level in the description of the polarisation, but we have to introduce the electron-hole interaction (in other words a non delta-like  $\Gamma$ ) through a second iteration of the Hedin equation<sup>28</sup>. This procedure allows to arrive to a Dyson equation for a generalised four point  $P$  (see ref.<sup>28</sup>, for details of the derivation), which describes the electron-hole dynamics and reads as:

$$P(1234) = P_{IQP}(1234) + \int P_{IQP}(1256)K(5678)P(7834)d(5678) \quad (21)$$

and it is known as the Bethe–Salpeter equation (BSE).  $P_{IQP}$  describes the propagation of independent quasi-electron and quasi-hole couples while all the interactions are contained in the Kernel  $K$ . The kernel  $K$  is made of two parts, deriving from the functional derivative of the Hartree potential and of the selfenergy with respect to the single-particle Green's function. So, using the GW approximation for  $\Sigma$  and neglecting both  $\delta W/\delta G$  and the dynamical effects in  $W$ , the kernel becomes<sup>28</sup>:

$$K(1234) = \delta(12)\delta(34)v(13) - \delta(13)\delta(24)W(12). \quad (22)$$

If we write the kernel in reciprocal space and eliminate the long range divergent contribution to  $v$  we can treat both the excitonic and the local fields effects at the same footing. In fact it can be shown<sup>28</sup> that the modified first term is taking care of the local fields effect, while the second represents the attractive screened electron-hole coulomb interaction. As we will see in the following examples the first term is particularly important in low dimensional systems, while the second one is, generally, the most important on bulk materials.

In practice, to solve the BSE, the problem is recast into an effective two-body hamiltonian form. To do this a basis of couples of LDA Bloch wavefunctions  $\phi_{nk}^{LDA}$  is employed. In this basis we have that the independent particle polarisation is:

$$P_{(n_1, n_2), (n_3, n_4)}^0 = \frac{(f_{n_2} - f_{n_1})\delta_{n_1, n_3}\delta_{n_2, n_4}}{\epsilon_{n_2} - \epsilon_{n_1} - \omega - i\eta}. \quad (23)$$

It can be show that ( see ref.<sup>29</sup> for all the mathematical details):

$$P = [1 + iP^0K]^{-1}P^0 = [H_{exc} - I\omega]_{(n_1, n_2), (n_3, n_4)}^{-1}(f_{n_4} - f_{n_3}) \quad (24)$$

where an effective excitonic hamiltonian, defined as the following, has been introduced:

$$H_{exc}^{(n_1, n_2), (n_3, n_4)} = (E_{n_2} - E_{n_1})\delta_{n_1, n_3}\delta_{n_2, n_4} - i(f_{n_2} - f_{n_1}) \times \\ \int d\mathbf{r}_1 d\mathbf{r}'_1 d\mathbf{r}_2 d\mathbf{r}'_2 \phi_{n_1}(\mathbf{r}_1) \phi_{n_2}^*(\mathbf{r}'_1) K(\mathbf{r}_1, \mathbf{r}'_1, \mathbf{r}_2, \mathbf{r}'_2) \phi_{n_3}^*(\mathbf{r}_2) \phi_{n_4}(\mathbf{r}'_2)$$

Hence, using the spectral representation <sup>29</sup> for the inverse of a matrix, the interacting polarisation can be obtained solving an effective eigenvalue problem:

$$\sum_{(n_3, n_4)} H_{exc}^{(n_1, n_2), (n_3, n_4)} A_\lambda^{(n_3, n_4)} = E_\lambda A_\lambda^{(n_1, n_2)}. \quad (25)$$

For the calculation of absorption spectra, we can limit ourselves to transitions with positive frequency<sup>28</sup>, i.e.  $(n_1, n_2)$  and  $(n_3, n_4)$  are pairs of one valence and one conduction band, respectively. Moreover, we build up the spectra of optical properties by considering only negligible momentum transfer, hence the same  $\mathbf{k}$  for the valence and the conduction state. In this way the macroscopic dielectric function, written in terms of the excitonic binding energies and eigenfunctions is:

$$\epsilon_M(\omega) = 1 + \lim_{\mathbf{q} \rightarrow 0} v(\mathbf{q}) \sum_\lambda \frac{\left| \sum_{v, c, \mathbf{k}} \langle v, \mathbf{k} - \mathbf{q} | e^{-i\mathbf{q}\mathbf{r}} | c, \mathbf{k} \rangle A_\lambda^{(v, c; \mathbf{k})} \right|^2}{(E_\lambda - \omega)}. \quad (26)$$

The calculation of  $\epsilon_M$  is generally very demanding because the excitonic hamiltonian matrix to be diagonalised can be very large. In fact the relevant parameters which determine its size are the number of  $\mathbf{k}$  points in the BZ, the number of the valence bands  $N_v$ , the number of conduction bands  $N_c$  which build the basis set of pairs of states.

BSE calculations, performed in insulators and semiconductors <sup>28,32,30,31</sup>, show how the inclusion of the electron-hole Coulomb interaction allows a quantitative comparison with experiments, not only below the electronic gaps, where generally bound excitons are formed, but also above the continuum edge. One of the first examples appeared in the literature is given by bulk silicon <sup>30</sup> where excitonic effects have been shown to enhance the E1 peak by almost 100%. Furthermore, the e-h interaction generally induces a redshift of the spectral peaks, which partially cancels the blueshift arising from the self-energy corrections. In the last ten years we assisted to a rapid growth of applications of this computational scheme to many materials from bulk semiconductors to real surfaces and nanostructures.

Here we concentrate on two applications of some silicon nanowires and on silicon nanoclusters.

#### 4.1. *Examples: Silicon nanowires (1D)*

In Fig.5 we report the imaginary part of the dielectric function of a Si [100] wire with a linear cross section of  $4\text{\AA}$  for light polarised along the growth axis and perpendicular to it. These spectra are calculated for an interwire distance (minimum distance between wire surfaces), equal to  $10\text{\AA}$ , which makes the interaction among wires negligible and for this reason we will refer to them as *isolated wires*. The first row of each panel shows the optical spectrum obtained at the RPA level, confirming essentially the results obtained in ref. <sup>33</sup>. The second row shows how the dielectric response is modified by taking into account the inhomogeneity of the system (RPA+LF). In particular, including the so called local-field effects, we observe a small change of the optical spectrum for light polarised along the wire axis, while we find an important intensity reduction for the perpendicular light polarisation (right panel). The reason that RPA, without LF, fails for  $\perp$  polarisation is due to the depolarisation effect <sup>34</sup> which is created by the polarisation charges induced in the system. The depolarisation is accounted only if LFs are included, and is responsible of the suppression of the low energy absorption peaks in  $\perp$  direction, rendering the wire almost transparent below 8 eV. A similar anisotropic behaviour, found in other first-principles calculations on nanotubes <sup>34,35</sup> and nanowires <sup>36,37</sup>, has been observed for the optical absorption of carbon nanotubes <sup>38</sup>, for the photoluminescence spectra of porous silicon <sup>39</sup> and for the optical gain in silicon elongated nanodots <sup>40</sup>.

The third row of each panel reports both the absorption spectra when self-energy corrections (GW) and self-energy, local-field and excitonic effects (GW+LF+EXC) are taken into account. For perpendicular light polarisation (right panel), the GW+LF+EXC spectrum is rather similar to the RPA+LF curve, whereas for parallel light polarisation, a big transfer of the oscillator strength to the low energy peaks is observed, together with a reduction of the Sommerfeld factor above the electronic gap (as predicted in simplified models <sup>41,42</sup>). Large exciton binding energies, due to the larger overlap of electron and hole wavefunctions inside the wire, come out.

How does the inter-wire distance affect the optical absorption? This point is of particular importance since experimentally, very often, the individual wires are close packed and can interact with each other via long-range forces induced by excitations.

In Fig.6 are reported the theoretical optical spectra calculated at the

$GW$  and at  $EXC + LF + GW$  level for different inter-wires distances:  $D_{w-w} = 10\text{\AA}$  top panel (isolated),  $D_{w-w} = 3\text{\AA}$  central panel (solid1),  $D_{w-w} = 1\text{\AA}$  bottom panel (solid2). Looking at left part of the three panels, we first note that the depolarisation effect decreases reducing the inter-wires distance. The packing makes the wire no more transparent for light polarised perpendicular to the axis. Moreover we observe that when the wires are very close to each other (solid2), the absorption for perpendicular light polarisation becomes more important with respect to the other polarisation. Another important effect can be seen reducing the inter-wires distance: a reduction of the opening of the DFT gaps, of the  $GW$  corrections, and also a reduction of the excitonic binding energy. In particular, looking at the top and central right panels, we observe that the spectra after the inclusion of all many-body effects are quite similar. This is probably due to the lack of local fields effects and to a strong confinement of excitons within each wire, with respect to the DFT electron states. As a consequence, excitons in different wires behave quite independently for this light polarisation. Only when the inter-wire distance is further reduced to about  $1\text{\AA}$  (solid2), a slight red-shift of the optical  $EXC + LF + GW$  spectrum starts to be visible.

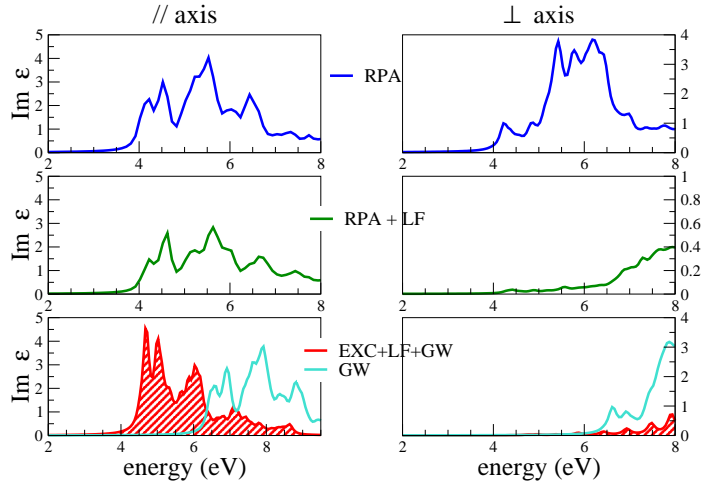


Figure 5. Imaginary part of the dielectric function of an isolated  $[100]$  SiNW (0.4 nm). Left panels: light polarised along the wire axis; right panels: light polarised perpendicularly to this axis.

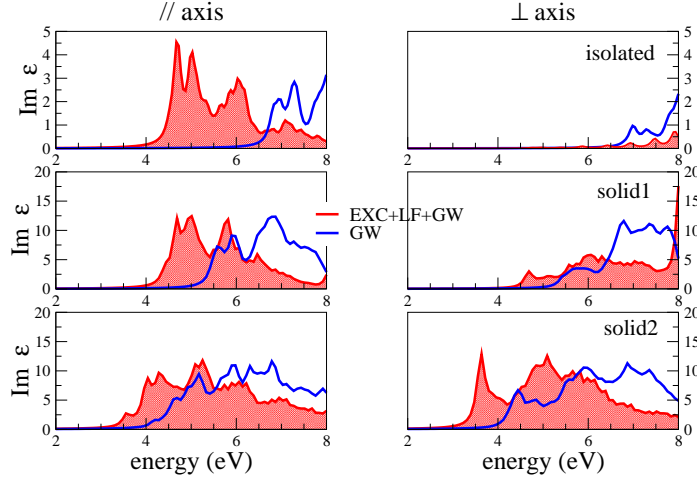


Figure 6. Imaginary part of the dielectric function of Si[100] wires:  $D_{w-w} = 10\text{\AA}$  (almost isolated), a solid of interacting nanowires with  $D_{w-w} = 3\text{\AA}$  (solid1), a solid of interacting nanowires with  $D_{w-w} = 1\text{\AA}$  (solid2)

#### 4.2. Example: silicon nanoclusters (0D)

Another example that shows the importance of introducing Many-Body effects in studying low dimensional systems is the emission and absorption spectra of Silicon nanocrystals (Si-nc). These have attracted increasing interest because of the possibility to engineer luminescing transitions in an otherwise indirect gap material<sup>44</sup>. It is generally accepted that the quantum confinement, caused by the restricted (nanometric) size, is essential for the visible light emission in Si nanostructures. Still the exact role of defects, doping, and interface structure in the photoluminescence (PL) spectra have to be clarified. In particular, the PL properties of embedded Si-nc in  $\text{SiO}_2$  suggest that oxygen induces important modifications in the electronic and optical properties of silicon nanocrystals<sup>45</sup>. In Fig.8 we show our calculated absorption and emission spectra for a small Si nanocluster, the  $\text{Si}_{10}\text{H}_{16}$ , and the corresponding optical spectra in the case of  $\text{Si}_{10}\text{H}_{14}\text{O}$ , where two hydrogen atoms have been substituted by a oxygen atom in a bridge configuration (see Fig.7). Absorption and emission are calculated in the ground and excited states respectively, where the excited state geometry corresponds to the electronic configuration in which the highest occupied single-particle state (HOMO) contains a hole ( $h$ ), while the lowest unoccupied single-particle state (LUMO) contains the corresponding electron ( $e$ ).

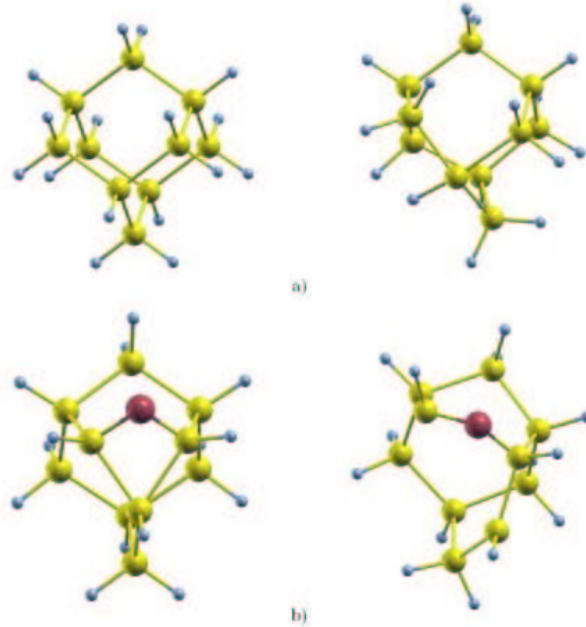


Figure 7. Geometries of a)  $Si_{10}H_{16}$  and b)  $Si_{10}H_{14}O$  nanoclusters. Left: ground state geometries; right: excited state geometries

Excitonic, local field and self-energy effects are included. A strong photoluminescence peak appears around 1.5 eV in the case of  $Si_{10}H_{14}O$ , due to a bound exciton with a large binding energy of  $\sim 2$  eV. The resulting emission spectrum well compares with the experimental spectrum of Ma et al.<sup>45</sup> shown in the inset. Our results suggests that the presence of a Si-O-Si bridge bond at the surface of Si-nc can explain the nature of luminescence in Si nanocrystallites embedded in  $SiO_2$ .

## 5. Conclusions

We have shown that parameter-free calculations of the spectroscopic properties of systems with different dimensionality and microscopic order, are now possible using Many-Body Perturbation Theory to correct the failures of the one-particle DFT approach. This scheme allows to determine both

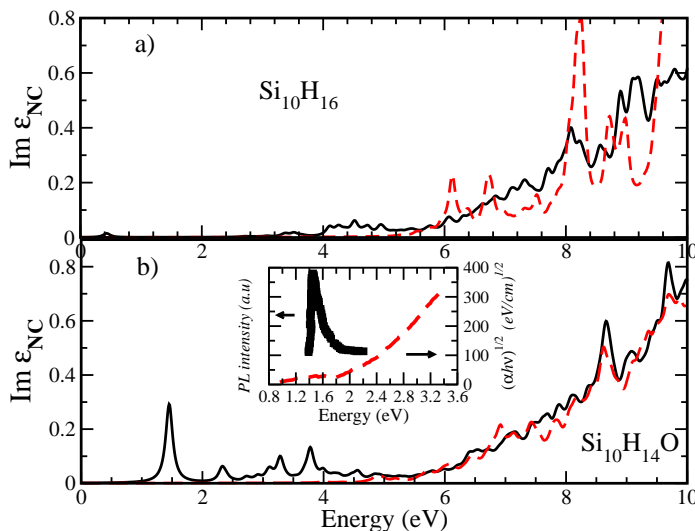


Figure 8. a) Imaginary part of the dielectric function of  $Si_{10}H_{16}$  nanocluster. Solid line: emission; dashed line: absorption. b) Imaginary part of the dielectric function of  $Si_{10}H_{14}O$  nanocluster. Solid line: emission; dashed line: absorption. Inset: experiment by Ma et al. <sup>45</sup>.

ground state and excited state properties at the same level of microscopic accuracy. We have discussed self-energy effects in the GW approximation which yields quite accurate results for the electronic gaps in many materials. Moreover, we have introduced the Bethe-Salpeter equation needed to describe the electron-hole interaction and showed some examples where theoretical response are strongly influenced by many body effects.

### Acknowledgments

This work has been supported by MIUR project PRIN NANOEXC 2005, MIUR project NANOSIM, by the EU through the Nanoquanta Network of Excellence (NMP4-CT-2004-500198) and by CNISM. Computer resources from INFN “Progetto Calcolo Parallelo” at CINECA are gratefully acknowledged.

### References

1. The DFT-GGA calculations have been performed using the FHI98MD code <sup>2</sup>, the PWSCF code: S. Baroni, S. de Gironcoli, A. Dal Corso, P. Gianozzi, <http://www.pwscf.org/>, and the ABINIT code <sup>3</sup> sX and HF calculations have been performed using VASP. GW and BSE calculation

have been performed using codes developed in the NANOQUANTA NoE  
<http://www.nanoquanta.eu>

2. M. Bockstedte, A. Kley, J. Neugebauer, and M. Scheffler, *Comp. Phys. Comm.* **107**, 187 (1997)
3. X. Gonze, J.-M. Beuken, R. Caracas, F. Detraux, M. Fuchs, G.-M. Rignanese, L. Sindic, M. Verstraete, G. Zerah, F. Jollet, M. Torrent, A. Roy, M. Mikami, Ph. Ghosez, J.-Y. Raty, D.C. Allan. *Computational Materials Science* 25, 478 (2002)
4. G. Onida, L. Reining, R. W. Godby, R. Del Sole, and W. Andreoni *Phys. Rev. Lett.* **75**, 818 (1995)
5. D. Varsano PhD Thesis, University of the Basque Country, San Sebastian, Spain, (2006)
6. C. A. Rozzi and D. Varsano and A. Marini and E. K. U. Gross and Angel Rubio, *Phys. Rev. B* **73**, 205119 (2006)
7. V. Garbuio et al., to appear in *Phys. Rev. Lett.*
8. P. Hohenberg and W. Kohn, *Phys. Rev.* **136**, B864 (1964).
9. R.M. Dreizler and E.K.U. Gross *Density Functional Theory* (Springer Verlag Hedelberg, 1990) R.O. Jones and O. Gunnarsson *Rev. Mod. Phys.* **61**, 689 (1989)
10. W. Kohn and L. J. Sham, *Phys. Rev.* **140**, A1113 (1965).
11. J.P. Perdew, K. Burke, and Y. Wang, *Phys. Rev. B* **54**, 16533 (1986)
12. J.P. Perdew, J.A. Chevary, S.H. Vosko, K.A. Jackson, M.R. Pederson, D.J.Singh, C. Fiolhais *Phys. Rev. B* **46**, 6671 (1992)
13. A. Seidl, A. Görling, P. Vogl, and J. Majewski *Phys. Rev. B* **53**, 3764 (1996)
14. K.C. Pandey, *Phys. Rev. B* **25**, R4338 (1982)
15. F. Bechstedt, A.A. Stekolnikov, J. Furthmüller, P. Käckell, *Phys. Rev. Lett.* **87**, 16103 (2001); A.A. Stekolnikov, J. Furthmüller and F. Bechstedt, *Phys. Rev. B* **65**, 115318 (2002)
16. A. Scholze, W.G. Schmidt, F. Bechstedt, *Phys. Rev. B* **53**, 13725 (1996)
17. G. Kern, J. Hafner, J. Furthmüller, G. Kresse, *Surf. Sci.* **357-358**, 422 (1995)
18. R. Graupner et al., *Phys. Rev. B* **55**, 10841 (1997)
19. F.J. Himpsel, D.E. Eastman, P. Heimann, J.F. van der Veen, *Phys. Rev. B* **24**, 7270 (1981)
20. R. W. Godby, M. Schlüter, and L. J. Sham, *Phys. Rev. Lett.* **56**, 2415-2418 (1986)
21. L. Hedin and S. Lundqvist, in *Solid State Physics*, Ed. H. Ehrenreich, F. Seitz, D. Turnbull (Academic, New York), Vol. 23, pag.1, (1969)
22. M.S. Hybertsen, S.G. Louie, *Phys. Rev. B* **34**, 5390 (1986)
23. R. W. Godby, M. Schlüter and L. J. Sham, *Phys. Rev. B* **37**, 10159 (1988)
24. L. Hedin, *Phys. Rev.* **139**, A796 (1965)
25. K. Laasonen et al., *J. Chem. Phys.* **99**, 9080 (1993)
26. see e.g. A. Bernas et al., *Chem. Phys.* **222**, 151 (1997) and ref. therein;  
<http://www.ensta.fr/muguet/papers/ECCC7/band.html> and ref. therein
27. F. Aryasetiawan, O. Gunnarsson, *Rep. Prog. Phys.* **61**, 237 (1998)
28. G. Onida, L. Reining, and A. Rubio, *Rev. Mod. Phys.* **74**, 601 (2002).
29. S. Albrecht, Ph. D. thesis, Ecole Polytechnique, France (1999).
30. S. Albrecht, L. Reining, R. Del Sole, and G. Onida *Phys. Rev. Lett.* **80**,

- 4510-4513 (1998)
31. L. X. Benedict, E. L. Shirley, and R. B. Bohn Phys. Rev. Lett. **80**, 4514-4517 (1998)
  32. M. Rohlfing and S. G. Louie Phys. Rev. Lett. **81**, 2312-2315 (1998)
  33. A. N. Kholod, V. L. Shaposhnikov, N. Sobolev, V. E. Borisenko, F. A. D'Avitaya, S. Ossicini, Physical Review B 70 (2004) 035317.
  34. A. G. Marinopoulos, L. Reining, A. Rubio, N. Vast, Phys. Rev. Lett. **91**, 046402 (2003).
  35. E. Chang, G. Bussi, A. Ruini, E. Molinari, Phys. Rev. Lett. **92**, 196401 (2004).
  36. M. Bruno, M. Palumbo, A. Marini, R. Del Sole, V. Olevano, A. N. Kholod, and S. Ossicini, Phys. Rev. B **72**, 153310 (2005).
  37. F. Bruneval, S. Botti, and L. Reining, Phys. Rev. Lett. **94**, 219701 (2005).
  38. N. Wang and *et. al.*, Nature **408**, 50 (2000)
  39. D. Kovalev, B. Averboukh, M. Ben-Chorin, and F. Koch, Al. L. Efros and M. Rosen, Phys. Rev. Lett. **77**, 2089 (1996) (1996).
  40. M. Cazzanelli and D. Kovalev and L. Dal Negro and Z. Gaburro and L. Pavesi, Phys. Rev. Lett. **93**, 207402 (2004)
  41. T. Ogawa, T. Takagahara, Phys. Rev. **43** 14325 (1991) .
  42. T. Ogawa, T. Takagahara, Phys. Rev. B **44** 8138 (1991).
  43. S. Baroni, A. Dal Corso, S. de Gironcoli, <http://www.pwscf.org>.
  44. S. Ossicini, L. Pavesi, F. Priolo, in *Light Emitting Silicon for Microphotonics*, Springer Tracts in Modern Physics, 194, Berlin (2003) .
  45. Z. Ma, X. Liao, G. Kong, J. Chu, Applied Physics Letter 75 (1999) 1857.